DOI: 10.1002/ejic.200900101

# Tuning Electronic Properties of Biomimetic [2Fe-2S] Clusters by Ligand Variations

**Joachim Ballmann,[a] Sebastian Dechert,[a] Serhiy Demeshko,[a] and Franc Meyer*[a]**

**Keywords:** Ligand effects / Bioinorganic chemistry / Iron / Sulfur / S ligands

Electronic effects of coordinated thiolate ligands on biomimetic [2Fe-2S] cluster cores have been examined by using three 2,2′-dithiobiphenyl chelate ligands that differ by the backbone substituents (Cl, H, *t*Bu). While the X-ray crystallographic analyses show little structural variation and Mössbauer spectra reveal only subtle differences for the three complexes **1**–**3**, superconducting quantum interference device (SQUID) magnetic data and UV/Vis spectroscopy in solution demonstrate that the different ligand environments cause significant electronic changes in the cluster cores. In particular, potentials for the one-electron reduction differ drastically over almost 0.5 V among the series. Due to the tight chelate arrangement, the reduced mixed-valent species are relatively stable on the electrochemical time scale, which is unusual for all-S-ligated [2Fe-2S] systems. The set of new complexes **1**–**3** thus provides a valuable platform to investigate reactivity patterns and the effect of electronic variations in biomimetic [2Fe-2S] clusters.


## Introduction

Iron-sulfur clusters that contain a core of iron atoms and inorganic sulfide are ubiquitous natural cofactors. They are involved in a variety of fundamental enzymatic processes that are of crucial importance in biological systems.[1] In addition to electron transfer, which is regarded as their primary biological role, some exciting and much more versatile functions of iron-sulfur clusters have been discovered over the last decade. These comprise, inter alia, catalysis,[2] sensing of small molecules,[3] SAM-radical-based processes[4] (SAM = *S*-adenosylmethionine) and gene regulation.[5] Iron-sulfur clusters are thus no longer seen as electron-transfer sites only, but are now referred to as nature's modular multipurpose structures.[1b] These clusters can be perceived as molecular $Fe_xS_y$ systems stabilized by protein ligands, mostly S-bound cysteinato residues. Surprisingly, most studies on synthetic Fe-S clusters focus on intrinsic properties of the cluster cores,[6] but little attention has been paid to variations of cluster properties that arise from the modulating effect of the ligands. While synthetic models that emulate structural characteristics and some spectroscopic characteristics of the most common biological iron-sulfur clusters are well established,[6] systematic analyses that correlate the substitution pattern of the ligand with the electronic signatures of the central core are largely unavailable, in particular for the smallest clusters, the [2Fe-2S] systems. It should be noted that the electrostatic environment surrounding the iron-sulfur cluster is assumed to play a major role in determining the redox potential of [2Fe-2S] ferredoxins, which may vary over a wide range.[7] Furthermore, the availability of a series of biomimetic [2Fe-2S] compounds with different electronic features is essential for emulating and understanding reactivity patterns related to the novel biological functions mentioned above. In this context, the present contribution focuses on ligand effects in all-S-ligated [2Fe-2S] clusters, chosen to mimic the biological first-sphere S-cysteine environment of [2Fe-2S] ferredoxins.

Almost all of the hitherto known and well-characterized all-S-ligated [2Fe-2S] clusters bear monodentate terminal ligands (mostly thiophenolate derivatives), but their further use is limited by their sensitivity and by the instability of the one-electron reduced species (due to formation of [4Fe-4S] clusters upon reduction). The most prominent exception and one of the best studied [2Fe-2S] clusters is the *o*-xylyl–$S_2$-ligated ferredoxin analogue, $(NBu_4)_2[Fe_2S_2(SCH_2\text{-}C_6H_4\text{-}CH_2S)_2]$, introduced by Holm and co-workers.[8] Its seven-membered chelate rings stabilize the system to an extent that decomposition upon electrochemical reduction is negligible on the timescale of the cyclic voltammetry experiment. Assuming that seven-membered chelate rings in general afford relatively stable [2Fe-2S] clusters, we intended to transfer this motive to thiophenolate-coordinated clusters by applying a series of 2,2′-dithiobiphenyl ligands.[9] The major aim was to modulate the ligand properties by means of electron-withdrawing or electron-donating backbone substituents, without changing the intimate overall cluster topology. Accordingly, three biphenyl-based ligands with electroni-

[a] Institut für Anorganische Chemie, Georg-August-Universität, Tammannstrasse 4, 37077 Göttingen, Germany
Fax: +49-551-39-3063
E-mail: franc.meyer@chemie.uni-goettingen.de
Supporting information for this article is available on the WWW under http://dx.doi.org/10.1002/ejic.200900101.

  

cally different substituents in the 3,3′,5 and 5′-positions (Cl, H, *t*Bu) were introduced as capping ligands at the cluster core, affording the new compounds **1**, **2** and **3** (see Scheme 1). Structural and electronic characteristics of **1**–**3** are discussed in view of the different properties of the peripheral R groups.

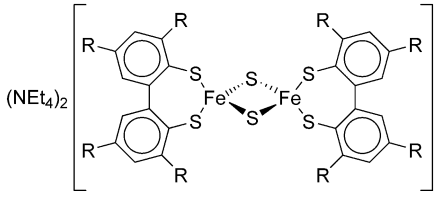


Scheme 1. [2Fe-2S] clusters **1**–**3** with electronically different biphenyl-based ligands described is this work.

## Results and Discussion

Clusters **1** and **3** were synthesized by standard salt metathesis reactions, starting from $(NEt_4)_2[Fe_2S_2Cl_4]$,[10] whereas **2** was more conveniently obtained via a ligand exchange pathway, starting from the indolate-ligated precursor $(NEt_4)_2[Fe_2S_2(indolate)_4]$[11] (the existence of **2** was previously mentioned in the literature,[12] but neither a synthetic procedure nor any spectroscopic data were reported). An alternative synthesis of **1** by using the ligand exchange approach is possible as well and is described in the Experimental Section. Compounds **1** and **2** were isolated in good yields (>50%), **3**, however, only in 23%, possibly due to the bulky *tert*-butyl *ortho* substituents that disfavour the coordination of two ligands to a single cluster core. Single crystals suitable for X-ray diffraction were grown for all three complexes by slow diffusion of $Et_2O$ into MeCN solutions of the isolated and purified compounds (see ORTEP plots in Figure 1). All three cluster complexes crystallize as (*pseudo*-) $C_{2h}$ symmetric molecules with the $C_2$ axis through both iron atoms and the perpendicular mirror plane through the bridging sulfides. Thus, one of the 2,2′-dithiobiphenyl ligands in each cluster is axial-*R* and the other axial-*S* configured. Most likely these *meso*-compounds preferably crystallize, whereas the *RR*,*SS* pairs precipitate as microcrystalline powders or remain dissolved until internal racemization to the *RS*,*SR*-*meso* pairs takes place.

Accidentally, few crystals of the dianion of **1** with one $NEt_4^+$ and one $Cp_2Co^+$ counterion (**1′**) were obtained from a preliminary reduction experiment (which was intended to afford the corresponding mixed-valent species, with cobaltocene as reductant). Compound **1′** crystallizes in $C_1$ symmetry; both ligands are axial-*R* or axial-*S* configured (see Figure 2; independent *RR*- and *SS*-enantiomers are present in the asymmetric unit, related by a mirror plane). This supports the assumption that both the $C_{2h}$ and $C_1$ isomers are present, but crystallization of only one of them – usually the *meso* diastereomer – is favoured, at least with two $NEt_4^+$ counterions.

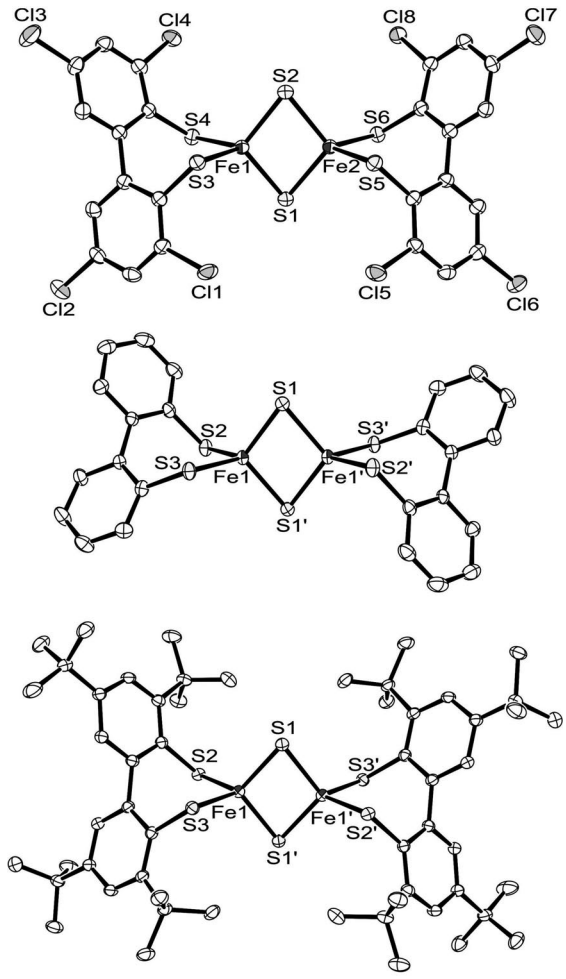


Figure 1. ORTEP plots (50% probability thermal ellipsoids) of the molecular structures of **1** (top), **2** (middle) and **3** (bottom). The $NEt_4^+$ counterions and all hydrogen atoms have been omitted for clarity. Key structural parameters are summarized in Table 1.

Although eight chlorine atoms in **1** or eight *tert*-butyl groups in **3** are expected to significantly influence the electronic structure of the central [2Fe-2S] core as compared to parent **2**, only minor structural changes of the corresponding core geometries[13] are observed (prominent atom distances and angles are summarized in Table 1). Thus, the Fe···Fe distances in **1** and **2** are very similar (ca. 2.67 Å), while a slightly elongated intermetallic distance is found in **3** (2.72 Å). Accordingly, the bond lengths to the bridging sulfides (2.21 Å) and the angles Fe–(μ-S)–Fe at those sulfides (75.9°) are also increased to some extent in **3**. Ligand bite angles RS–Fe–SR, distances to the terminal thiolates Fe–SR and geometric distortions at the iron sites (semiquantified by $\tau_4$ values)[14] are in a similar range for all three clusters.

In order to find out whether the ligand substitutions indeed do affect the electronic properties of the cluster cores, regardless of their rigid geometry, all new complexes were characterized in solution by several spectroscopic methods. Positive and negative ion ESI mass spectrometry proved to be a valuable analytical tool to confirm formation and in-

  

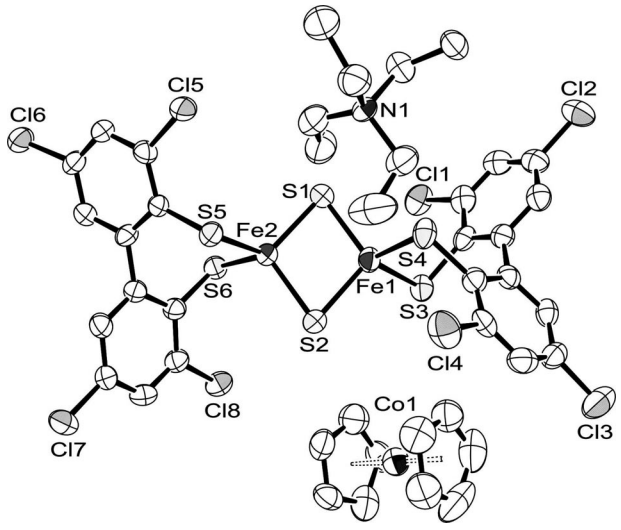


Figure 2. ORTEP plot (50% probability thermal ellipsoids) of the molecular structure of $(NEt_4)(Cp_2Co)[Fe_2S_2(3,3',5,5'$-tetrachloro-1,1′-biphenyl-2,2′-dithiolate)$_2]$ (**1′**). All hydrogen atoms are omitted for clarity. Selected interatomic distances and angles are summarized in Table 1.

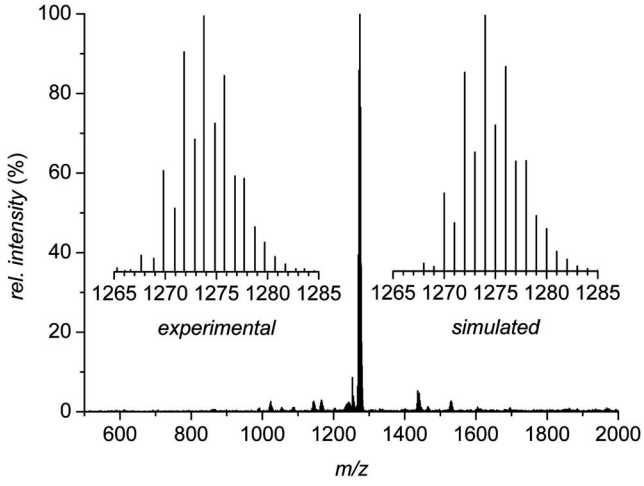


Figure 3. Positive-ion ESI-MS spectrum of **1** in MeCN solution. The insets show the experimental and expected isotopic distribution pattern for $[M + NEt_4]^+$.

Table 1. Selected structural parameters for clusters **1**, **1′**, **2** and **3**. Interatomic distances are given in Å and angles in °.

| Compound | **1** | **1′** | **2** | **3** |
|---|---|---|---|---|
| Fe···Fe | 2.6748(7) | 2.6936(14) | 2.6722(4) | 2.7212(5) |
| Fe–SR | 2.3080(8) | 2.3111(19) | 2.2864(4) | 2.3002(5) |
| | 2.3051(7) | 2.318(2) | 2.2989(4) | 2.2983(5) |
| | 2.3121(8) | 2.301(2) | 2.2864(4) | 2.3002(5) |
| | 2.3112(8) | 2.3239(18) | 2.2989(4) | 2.2983(5) |
| Fe–(μ-S) | 2.1964(7) | 2.187(2) | 2.2094(5) | 2.2113(5) |
| | 2.1925(7) | 2.2004(18) | 2.1969(5) | 2.2152(5) |
| | 2.2010(7) | 2.1952(18) | 2.2094(5) | 2.2113(5) |
| | 2.2037(7) | 2.219(2) | 2.1969(5) | 2.2152(5) |
| RS–Fe–SR | 103.51(3) | 104.89(7) | 103.684(16) | 104.735(18) |
| | 105.55(3) | 105.33(7) | 103.684(16) | 104.735(18) |
| Fe–(μ-S)–Fe | 74.93(3) | 75.85(6) | 74.665(15) | 75.866(16) |
| | 74.95(2) | 75.11(6) | 74.665(15) | 75.866(16) |
| $\tau_4$ | 0.874 | 0.926 | 0.878 | 0.884 |
| | 0.895 | 0.920 | 0.878 | 0.884 |

tactness of the anticipated complexes, since spectra of MeCN solutions show dominant signals for $[Fe_2S_2L_2(NEt_4)_3]^+$ and $[Fe_2S_2L_2(NEt_4)]^-$, respectively (the positive-ion ESI spectrum of **1** is shown in Figure 3 as an example).

The absence of possible diamagnetic impurities (e.g. free ligands) was proven by proton NMR spectroscopy in $[D_3]$-MeCN at room temperature. Due to the strong antiferromagnetic coupling between the two iron atoms (as generally observed in synthetic [2Fe-2S] clusters), reasonably resolved but broadened signals were recorded for **1**–**3**, with dominant $NEt_4^+$ resonances in the aliphatic regime and characteristic signals for the aromatic 4,4′,6,6′-protons at approximately 9 and 10 ppm. In MeCN solution, each complex exhibits three distinct UV/Vis absorption bands at 330–350 nm, 420–450 nm and 520–550 nm (for **2** and **3** additional shoulders or bands are observed at 370 nm and 383 nm, respectively). A redshift of the transitions of lowest energy in the series **1** (523 nm) < **2** (547 nm) < **3** (550 nm) indicates their largely thiophenolate-to-core charge-transfer character, since electron-donating substituents like the *tert*-butyl moieties in **3** are expected to lower the transition energies for these LMCT bands. No clear trend is apparent for the bands at 330–350 and 420–450 nm, however, which suggests that the latter absorption bands involve charge-transfer transitions from both the bridging inorganic sulfides and terminal thiophenolates to the ferric iron atoms (see Figure 4). Redox potentials of all clusters were studied by cyclic voltammetry in MeCN solution at room temperature (with the $Cp_2^*Fe/Cp_2^*Fe^+$ couple as internal standard). Reduction is electrochemically reversible (or almost reversible) at a scan rate of 100 mV/s, which is quite remarkable since most other all-S-ligated $[2Fe\text{-}2S]^+$ cores decompose rapidly at room temperature. The parent compound **2** is reduced to the mixed-valent state at $E_{1/2}$ = –1.14 V, the low potential being typical for synthetic [2Fe-2S] ferredoxin models. In contrast, the electron-poor cluster core in **1** accepts an electron at a relatively high potential of –0.96 V, whereas the reduction wave of the electron-rich cluster core in **3** is shifted significantly to a more cathodic value and is found at –1.43 V (Figure 5). These pronounced differences reflect the influence of the electron-withdrawing or electron-donating ligand substituents (eight Cl atoms in **1** vs. eight σ-donating *tert*-butyl groups in **3**) that decrease or increase electron density at the core position, respectively. The trend in reduction potentials in the series $E_{1/2}$ (**1**) > $E_{1/2}$ (**2**) > $E_{1/2}$ (**3**) is thus fully in line with expectations.

Solid samples of **1**–**3** were additionally characterized by zero-field Mössbauer spectroscopy and temperature-dependent magnetic susceptibility measurements. Spectral fits to the Mössbauer data were obtained by using Lorentzian

  

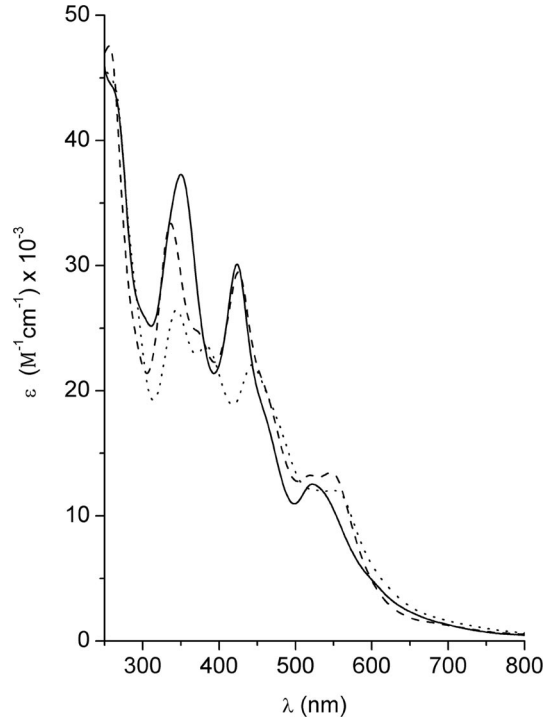


Figure 4. Electronic absorption spectra of **1** (solid line), **2** (dashed line) and **3** (dotted line) in MeCN solution.

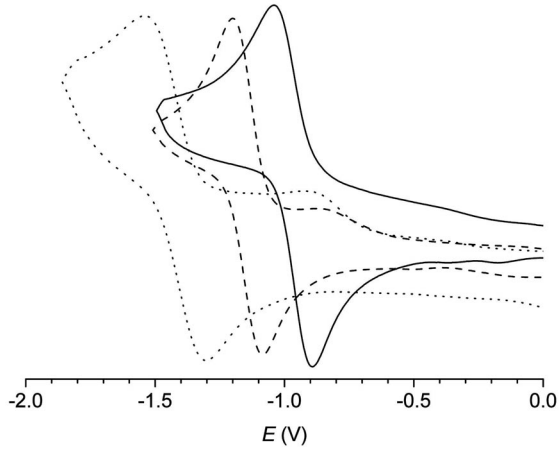


Figure 5. Cyclic voltammograms of **1** (solid line), **2** (dashed line) and **3** (dotted line) recorded in MeCN/0.1 M $NBu_4PF_6$ solution at a scan rate of 100 mV/s referenced vs. the $Cp_2^*Fe/Cp_2^*Fe^+$ couple.

line doublets with isomer shifts $\delta$ and quadrupole splittings $\Delta E_Q$ summarized in Table 2 (the spectrum of **2** is shown in Figure 6 as an example). Neither $\delta$ values nor $\Delta E_Q$ values show a clear trend when going from electron-withdrawing ligand substituents to electron-donating groups. Isomer shifts are almost identical at $\delta$ = 0.28 or 0.29 mm/s, and quadrupole splittings are found in the narrow range $\Delta E_Q$ = 0.82 ± 0.05 mm/s for all three cluster compounds. Thus, isomer shifts are in accordance with the ferric oxidation state $s$ = 2.825 ± 0.05 (calculated from the empirical correlation $\delta$ = 1.43 – 0.40 $s$ between oxidation state $s$ and $\delta$ that is valid for tetrahedral {$FeS_4$} sites)[16] but do not reflect the electronic influences of the peripheral ligand sphere around the iron-sulfur core. In comparison to **2** ($\Delta E_Q$ = 0.86 mm/s) and **3** ($\Delta E_Q$ = 0.83 mm/s), complex **1** ($\Delta E_Q$ = 0.77 mm/s) exhibits a slightly lower quadrupole splitting, even though $\tau_4$ values (that semi-quantify distortions of the coordination polyhedra from a perfect tetrahedron) are very similar for the three clusters reported here. No clear explanation for this finding can be provided yet, but an involvement of solid-state effects might play a role. Dynamic processes in solution (e.g., interconversion of the ligand diastereomers) would likely attenuate and overwhelm those effects to give rise to the substitution-dependent properties of **1**–**3** described above.

Magnetic susceptibility measurements for compounds **1**–**3** were carried out at 0.5 T from 2 K to 295 K. Magnetic moments, $\mu_{eff}$, at room temperature are in the range 1.9–2.7 $\mu_B$ and decrease towards zero upon cooling, which indicates significant antiferromagnetic coupling as is commonly observed for the $Fe_2S_2$ core ($S$ = 0 ground state). Coupling constants, $J$, were determined by using a fitting procedure to the appropriate Heisenberg spin Hamiltonian for isotropic exchange coupling and are summarized in Table 2.[17] In contrast to the Mössbauer parameters $\delta$ and $\Delta E_Q$, coupling constants, $J$, obtained from superconducting quantum interference device (SQUID) data clearly show a considerable trend, i.e. $|J|$ values decrease in the series **1** > **2** > **3**. As these parameters are expected to correlate with the Fe···Fe separations and the Fe–(μ-S)–Fe angles, a distinct trend, **1** ≈ **2** > **3**, might have been predicted on the basis of the molecular structures, since nearly identical core geometries for **1** and **2** are evident from X-ray diffraction analysis. Thus, results from both techniques that require solid-state samples – Mössbauer spectroscopy and magnetic susceptibility measurements – are not in full accordance with common expectations. As microcrystalline batch samples were used in these experiments, the most likely explanation is that some *RR*,*SS*-configured form is present in the batch samples of **1**–**3**, in addition to the crystalline *RS*,*SR* diastereomer. Since crystallization of the *RS*,*SR*-*meso* pairs is persistently accompanied by the precipitation of some microcrystalline material, but crystals of the *RR*,*SS* pairs were not obtained for any of the $NEt_4^+$ salts of complexes **1**–**3**, subtle structural differences between the two diastereomeric forms and their possible implications for spectroscopic and analytical data cannot be evaluated. Line width parameters from the Mössbauer spectra of **1**–**3** do not indicate the presence of additional cluster species (like the *RR*,*SS* forms) with significantly different coordination environments at the iron atoms. It should be noted, however, that the mixed $NEt_4^+/Cp_2Co^+$ salt, *RR*,*SS*-**1′**, exhibits an elongated Fe···Fe separation of 2.6936(14) Å [compared to the *RS*,*SR* diastereomer **1**: *d*(Fe···Fe) = 2.6748(7) Å], which confirms that certain structural variations may exist for the different diastereomers.

  

Table 2. Spectroscopic and electrochemical data for **1**–**3**.

| Compound | $\delta$ [$\Delta E_Q$] (mm/s)[a] | $\lambda_{max}$ (nm) [$\varepsilon$ ($M^{-1}cm^{-1}$)][b] | $J$ ($cm^{-1}$)[c] | $E_{1/2}$ (V)[d] |
|---|---|---|---|---|
| **1** | 0.28 [0.77] | 260 [sh, ca. 44500], 350 [ca. 37200], 424 [30000], 523 [12500] | –180 | –0.96 |
| **2** | 0.28 [0.86] | 257 [ca. 47500], 336 [ca. 33400], 425 [29500], 520 [13250], 547 [13500] | –158 | –1.14 |
| **3** | 0.29 [0.83] | 260 [sh, ca. 45000], 345 [26500], 383 [23600], 443 [22000], 550 [sh, 12000] | –141 | –1.43[e] |

[a] $^{57}$Fe Mössbauer parameters at 80 K, relative to Fe metal at room temperature. [b] Recorded in MeCN solution at room temperature. [c] Values obtained from fits to SQUID data. [d] Half-wave potential of the (quasi)-reversible process in MeCN/0.1 M $[NBu_4]PF_6$ at a scan rate of 100 mV/s vs. the $Cp^*_2Fe/Cp^*_2Fe^+$ couple. [e] Potential determined in MeCN/0.1 M $[NBu_4]PF_6$ solution at a scan rate of 100 mV/s vs. the $Cp_2Fe/Cp_2Fe^+$ couple is –1.94 V, corresponding to –1.43 V vs. the $Cp^*_2Fe/Cp^*_2Fe^+$ couple.[15]

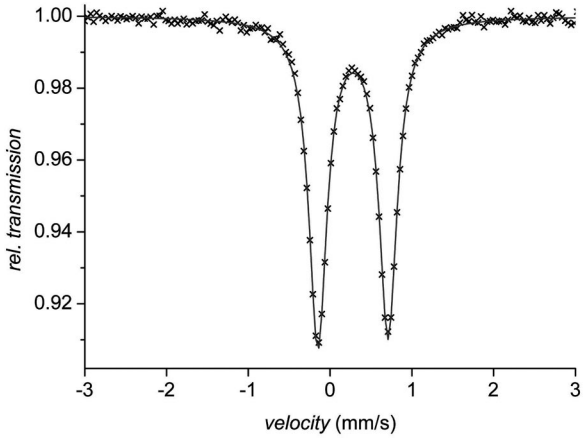


Figure 6. Zero-field Mössbauer spectrum of **2** recorded at 80 K. The curve is fitted to the experimental values (crosses) with $\delta$ = 0.28 mm/s and $\Delta E_Q$ = 0.86 mm/s.

## Conclusions

In summary, three new [2Fe-2S] ferredoxin model complexes with chelating capping ligands of the 2,2′-dithiolato-1,1′-biphenyl type have been prepared and fully characterized. The chelate backbone imparts a relatively high stability to the cluster cores, which allows reversible electrochemical reduction to the mixed-valent $[2Fe\text{-}2S]^+$ species even at room temperature. Systematic variation of electronic properties has been achieved by attaching either electron-withdrawing (Cl) or electron-donating substituents (*t*Bu) at the parent ligand framework, resulting in significant differences of the properties of the clusters despite substantial structural invariance. In particular, electron-withdrawing Cl substituents lower the total electron density at the cluster cores and cause a drastic anodic shift of the corresponding half-wave potentials for the $[2Fe\text{-}2S]^{2+}/[2Fe\text{-}2S]^+$ couple, thus facilitating reduction of the diferric species. While subtle differences in Mössbauer spectra are discernible and more pronounced differences are apparent in the SQUID data but remain unexplained, observed UV/Vis spectroscopic characteristics in solution reflect the expected trend. The series of new complexes **1**–**3** provides a valuable platform to investigate reactivity patterns of biomimetic [2Fe-2S] clusters and the effect of electronic variations. Since the full characterization of mixed-valent $[2Fe\text{-}2S]^+$ ferredoxin analogues is generally considered as a pending task in Fe-S chemistry to be achieved by synthetic bioinorganic chemists, future efforts will also focus on the preparative chemical reduction of electron-deficient all-S-ligated clusters. In this respect, the strategy presented here may be advanced further towards a perfluorinated 2,2′-dithio-1,1′-biphenyl ligand derivative, which will likely shift the cluster redox potential even more anodically, i.e., into the more biorelevant regime that is expected to allow isolation of the otherwise unstable $[2Fe\text{-}2S]^+$ core.

## Experimental Section

**General Considerations:** All manipulations were carried out under an anaerobic and anhydrous atmosphere of dry nitrogen by employing standard Schlenk techniques or in a glove box. $Et_2O$ was dried with sodium benzophenone ketyl, THF over potassium benzophenone ketyl, MeCN and $[D_3]$MeCN over $CaH_2$ and distilled prior to use. Glassware was dried at 120 °C overnight. $^1$H NMR spectra were recorded with a Bruker Avance 500 MHz spectrometer at room temperature. Chemical shifts are reported in ppm relative to residual proton signals of $[D_3]$MeCN at $\delta$ = 1.95 ppm. Microanalyses were performed by the "Analytisches Labor des Instituts für Anorganische Chemie der Universität Göttingen". UV/Vis spectra were recorded with an Analytik Jena Specord S 100 by using Schlenk quartz cuvettes. Mössbauer spectra were recorded with an alternating constant-acceleration spectrometer. Isomer shifts are given relative to iron metal at ambient temperature. Temperature-dependent magnetic susceptibilities of powdered samples were measured by using a SQUID magnetometer (MPMS-5, Quantum Design) at 0.5 T. Cyclic voltammetry was performed with a potentiostat/galvanostat Perkin–Elmer Model 263A with a glassy carbon working electrode and platinum reference and counterelectrodes in MeCN/0.1 M $[NBu_4]PF_6$ solution at room temperature. Ferrocene or decamethylferrocene was used as internal standard. Compounds $(NEt_4)_2[Fe_2S_2Cl_4]$,[10b] $(NEt_4)_2[Fe_2S_2(indolate)_4]$,[11] 3,3′,5,5′-tetrachloro-2,2′-dithio-1,1′-biphenyl, 2,2′-dithio-1,1′-biphenyl and 3,3′,5,5′-tetrakis-*tert*-butyl-2,2′-dithio-1,1′-biphenyl were synthesized according to reported methods.[9] All other chemicals were used as purchased.

**Bis(tetraethylammonium) Bis[(3,3′,5,5′-tetrachloro-2,2′-dithiolato-1,1′-biphenyl)(μ-sulfido)ferrate(III)] (1)**

**Method A:** To a solution of 3,3′,5,5′-tetrachloro-2,2′-dithio-1,1′-biphenyl (0.74 g, 2.08 mmol) in THF (20 mL) was added solid KH (0.17 g, 4.18 mmol, purchased as a 60% dispersion in mineral oil, repetitively washed with hexanes and dried in vacuo prior to use) at room temperature, and the resulting mixture was stirred for 1 h (evolution of hydrogen was observed during the first 10 min after addition). Subsequently, the opaque yellow reaction phase was diluted with MeCN (60 mL), and solid $(NEt_4)_2[Fe_2S_2Cl_4]$ (0.60 g, 1.04 mmol) was added in one portion in a positive stream of dinitrogen. After stirring the dark brown reaction mixture for 24 h at

  

room temperature, all volatiles were removed under reduced pressure, and the obtained solid residue was briefly dried in vacuo. The product was extracted with MeCN (60 mL) under vigorous stirring for 4 h at room temperature, and the supernatant was transferred to a 250 mL Schlenk flask by cannula filtration. The dark red filtrate was diluted with $Et_2O$ (60 mL) and kept at –20 °C for 3 d. Initial product crystallization was observed during that time and completed by addition of further $Et_2O$ (20 mL) and storage at –20 °C for another 3 d. The crystalline powder was isolated by filtration, washed with $Et_2O$ (10 mL) and dried in vacuo to obtain the pure dark red target material (0.60 g, 0.53 mmol, 51%). $^1$H NMR (500 MHz, [D$_3$]MeCN): $\delta$ = 1.31 ($s_{br}$, 24 H, $NEt_4$), 3.24 ($s_{br}$, 16 H, $NEt_4$), 9.11 ($s_{br}$, 4 H, Ar-H), 9.81 ($s_{br}$, 4 H, Ar-H) ppm. MS (ESI+): *m*/*z* (%) = 1273 (100) $[M + NEt_4]^+$. MS (ESI–): *m*/*z* (%) = 1014 (100) $[M – NEt_4]^-$. UV/Vis (MeCN solution): $\lambda_{max}$ ($\varepsilon$, $M^{-1}cm^{-1}$) = 260 (sh, ca. 34000), 350 (ca. 25000), 424 (17800), 523 (6050) nm. $C_{40}H_{48}Cl_8Fe_2N_2S_6$ (1144.5): calcd. C 41.98, H 4.23, N 2.45; found C 42.79, H 4.66, N 2.69. HRMS (ESI+): calcd. for $C_{48}H_{68}Cl_8Fe_2N_3S_6$ 1269.9946; found 1269.9936.

**Method B:** A solution of 3,3′,5,5′-tetrachloro-2,2′-dithio-1,1′-biphenyl (0.30 g, 0.85 mmol) in THF (10 mL) was added to a stirred suspension of $(NEt_4)_2[Fe_2S_2(indolate)_4]$ (0.30 g, 0.33 mmol) in MeCN (40 mL) at room temperature, and the resulting reaction mixture was stirred for 6 h. The reaction volume was concentrated to ca. 20 mL, and the crude product solution was layered with $Et_2O$ (30 mL). After diffusion at room temperature (for ca. 2 d) and initial product crystallization, the mixture was kept at –20 °C overnight. Additional $Et_2O$ (10 mL) was added to the Schlenk flask, which was kept at –20 °C for another 24 h. Beautiful large deep red crystals were filtered off, washed with $Et_2O$ (10 mL) and dried for ca. 6 h in vacuo to afford the pure product (0.25–0.35 g, 0.22–0.26 mmol, 66–80%). Analytical data were identical with those for the product obtained by method A.

**Bis(tetraethylammonium) Bis[(2,2′-dithiolato-1,1′-biphenyl)(μ-sulfido)ferrate(III)] (2):** A 100 mL Schlenk flask was charged with a stirring bar, $(NEt_4)_2[Fe_2S_2(indolate)_4]$ (0.99 g, 1.00 mmol) and 2,2′-dithio-1,1′-biphenyl (0.48 g, 2.20 mmol) in a glove box, followed by addition of MeCN (50 mL). The resulting reddish purple suspension was stirred at room temperature for 20 h to afford a deep red solution, indicating complete conversion. Removal of the solvent and extraction of free indole with THF/$Et_2O$ (1:3, 12.5 mL THF/40 mL $Et_2O$) gave a homogeneous black powder. This crude product was washed again with $Et_2O$ (20 mL), stirred for 30 min in MeCN (40 mL) until complete dissolution and left to stand at –20 °C overnight. Additional $Et_2O$ (10 mL) was added to the MeCN solution, and the mixture was kept at –20 °C for further 24 h. Filtration, rinsing with $Et_2O$ (20 mL) and removal of traces of solvent overnight in vacuo afforded a microcrystalline powder of the product (0.60 g, 0.69 mmol, 69%). $^1$H NMR (500 MHz, [D$_3$]MeCN): $\delta$ = 1.18 ($s_{br}$, 24 H, $NEt_4$), 2.71 ($d_{br}$, 4 H, Ar-H), 3.09 ($s_{br}$, 16 H, $NEt_4$), 4.07 ($d_{br}$, 4 H, Ar-H), 9.85 ($s_{br}$, 4 H, Ar-H), 9.05 ($d_{br}$, 4 H, Ar-H) ppm. MS (ESI+): *m*/*z* (%) = 998 (100) $[M + NEt_4]^+$. MS (ESI–): *m*/*z* (%) = 488 (60) $[L_2Fe]^-$, 637 (100) $[M – NEt_4 – NEt_3]^-$, 738 (30) $[M – NEt_4]^-$. UV/Vis (MeCN solution): $\lambda_{max}$ ($\varepsilon$, $M^{-1}cm^{-1}$): 257 (ca. 47500), 336 (ca. 33400), 425 (29500), 520 (13250), 547 (13500) nm. HRMS (ESI+): calcd. for $C_{48}H_{76}Fe_2N_3S_6$ 996.3104; found 996.3101.

**Bis(tetraethylammonium) Bis[(3,3′,5,5′-tetrakis-*tert*-butyl-2,2′-dithiolato-1,1′-biphenyl)(μ-sulfido)ferrate(III)] (3):** To a solution of 3,3′,5,5′-tetrakis-*tert*-butyl-2,2′-dithio-1,1′-biphenyl (1.20 g, 2.71 mmol) in THF (40 mL) at 0 °C was added dropwise *n*BuLi (1.80 mL, 3.0 M solution in hexanes, 5.42 mmol) and the resulting slightly yellow solution stirred for 1 h at 0 °C. This solution of the deprotonated ligand was cooled to –40 °C prior to rapid addition of a pre-cooled (0 °C) solution of $(NEt_4)_2[Fe_2S_2Cl_4]$ (0.75 g, 1.30 mmol) in MeCN (100 mL). The resulting reaction mixture was stirred for 1 h while the temperature was slowly raised to –30 °C and finally warmed to room temperature. All volatiles were removed in vacuo and the residual crude product extracted with THF (200 mL) under vigorous stirring for 30 min. After filtration, the reddish brown THF filtrate was condensed to a volume of ca. 80 mL, $Et_2O$ (100 mL) was added, and the mixture was kept at –20 °C overnight. Small amounts (ca. 50 mg) of an unidentified precipitate were filtered off and discarded prior to addition of further $Et_2O$ (200 mL) and pentane (100 mL). Subsequent cooling to –80 °C for 3 d caused product precipitation. Filtration, rinsing with $Et_2O$ (40 mL) and drying overnight in vacuo afforded the product (0.40 g, 0.30 mmol, 23%) as a red-brown powder. $^1$H NMR (500 MHz, [D$_3$]MeCN): $\delta$ = 1.18 ($s_{br}$, 24 H, $NEt_4$), 1.48 ($s_{br}$, 36 H, 5,5′-*t*Bu), ca. 2.0 ($s_{br}$, 3,3′-*t*Bu, overlapping with residual [D$_3$]-MeCN resonances), 3.11 ($s_{br}$, 16 H, $NEt_4$), 8.95 ($s_{br}$, 4 H, Ar-H), 9.91 ($s_{br}$, 4 H, Ar-H) ppm. MS (ESI+): *m*/*z* (%) = 1345 (100) $[M – C_2H_6]^+$, 1446 (75) $[M + NEt_4]^+$. MS (ESI–): *m*/*z* (%) = 937 (100) $[L_2Fe]^-$, 1186 (30) $[M – NEt_4]^-$. UV/Vis (MeCN solution): $\lambda_{max}$ ($\varepsilon$, $M^{-1}cm^{-1}$): 260 (sh, ca. 45000), 345 (26500), 383 (23600), 443 (22000), 550 (sh, 12000) nm. HRMS (ESI+): calcd. for $C_{72}H_{120}Fe_2N_2S_6$ 1317.6552; found 1317.6550.

CCDC-718009, -718010, -718011, -718012 contain supplementary crystallographic data. These data can be obtained free of charge from The Cambridge Crystallographic Data Centre via http://www.ccdc.cam.ac.uk/data_request/cif.

**Supporting Information** (see footnote on the first page of this article): Additional compound characterization data [ESI mass spectra, HRMS ESI(+) spectra, $^1$H NMR spectra, Mössbauer spectra and magnetic susceptibility measurements] and crystallographic data for all new compounds.

## Acknowledgments

We sincerely thank Jörg Teichgräber for collecting the CV data and Dr. Eckhard Bill (Max-Planck-Institut für Bioanorganische Chemie, Mülheim an der Ruhr, Germany) for preliminary Mössbauer measurements. Financial support by the DFG (International Research Training Group GRK 1422 "Metal Sites in Biomolecules: Structures, Regulation and Mechanisms"; see http://www.biometals.eu) and the Fonds der Chemischen Industrie (Kekulé fellowship for J. B.) is gratefully acknowledged.

[1] a) M. Fontecave, *Nature Chem. Biol.* **2006**, *2*, 171–174; b) H. Beinert, R. H. Holm, E. Münck, *Science* **1997**, *277*, 653–659; c) H. Beinert, *J. Biol. Inorg. Chem.* **2000**, *5*, 2–15.
[2] D. H. Flint, R. M. Allen, *Chem. Rev.* **1996**, *96*, 2315–2334.
[3] a) H. Ding, B. Demple, *Proc. Natl. Acad. Sci. USA* **1997**, *94*, 8445–8449; b) P. Gaudu, B. Weiss, *Proc. Natl. Acad. Sci. USA* **1996**, *93*, 10094–10098; c) E. Hidalgo, J. M. Bollinger Jr, T. M. Bradley, C. T. Walsh, B. Demple, *J. Biol. Chem.* **1995**, *270*, 20908–20914.
[4] a) M. Lotierzo, B. T. S. Bui, D. Florenti, F. Escalettes, A. Marquet, *Biochem. Soc. Trans.* **2005**, *33*, 820–823; b) R. W. Busby, J. P. M. Schelvis, D. S. Yu, G. T. Babcock, M. A. Marletta, *J. Am. Chem. Soc.* **1999**, *121*, 4706–4707.
[5] a) M. Hentze, L. C. Kühn, *Proc. Natl. Acad. Sci. USA* **1996**, *93*, 8175–8182; b) J. Rudolf, V. Makrantoni, W. J. Ingledew, M. J. R. Stark, M. F. White, *Mol. Cell* **2006**, *23*, 801–808; c) E. J. Merino, A. K. Boal, J. K. Barton, *Curr. Opin. Chem. Biol.* **2008**, *12*, 229–237.

  

[6] P. V. Rao, R. H. Holm, *Chem. Rev.* **2004**, *104*, 527–559.

[7] F. Capozzi, S. Ciurli, C. Luchinat, *Structure and Bonding, Vol. 90*, Springer-Verlag Berlin Heidelberg, **1998**, p. 127–160.

[8] a) J. J. Mayerle, S. E. Denmark, B. V. DePamphilis, J. A. Ibers, R. H. Holm, *J. Am. Chem. Soc.* **1975**, *97*, 1032–1045; b) B. K. Teo, R. G. Shulman, G. S. Brown, A. E. Meixner, *J. Am. Chem. Soc.* **1979**, *101*, 5624–5631; c) O. Gillum, R. B. Frankel, S. Foner, R. H. Holm, *Inorg. Chem.* **1976**, *15*, 1095–1100; d) J. G. Reynolds, R. H. Holm, *Inorg. Chem.* **1980**, *19*, 3257–3260; e) P. K. Mascharak, G. C. Papaefthymiou, R. B. Frankel, R. H. Holm, *J. Am. Chem. Soc.* **1981**, *103*, 6110–6116.

[9] J. Ballmann, M. G. G. Fuchs, S. Dechert, M. John, F. Meyer, *Inorg. Chem.* **2009**, *48*, 90–99.

[10] a) G. B. Wong, M. A. Bobrik, R. H. Holm, *Inorg. Chem.* **1978**, *17*, 578–584; b) Y. Do, E. D. Simhon, R. H. Holm, *Inorg. Chem.* **1983**, *22*, 3809–3812.

[11] J. Ballmann, X. Sun, S. Dechert, B. Schneider, F. Meyer, *Dalton Trans.*, DOI: 10.1039/B901242G.

[12] P. Beardwood, J. F. Gibson, *J. Chem. Soc., Dalton Trans.* **1983**, 737–748.

[13] L. E. Maelia, S. A. Koch, *Inorg. Chem.* **1986**, *25*, 1896–1904.

[14] L. Yang, D. R. Powell, R. P. Houser, *Dalton Trans.* **2007**, 955–964.

[15] a) N. G. Connelly, W. E. Geiger, *Chem. Rev.* **1996**, *96*, 877–910; b) J. R. Aranzaes, M.-C. Daniel, D. Astruc, *Can. J. Chem.* **2006**, *84*, 288–299.

[16] a) G. N. Schrauzer, V. P. Mayweg, H. W. Flick, W. Heinrich, *J. Am. Chem. Soc.* **1966**, *88*, 4604–4609; b) J. T. Hoggins, H. Steinfink, *Inorg. Chem.* **1976**, *15*, 1682–1685.

[17] A Hamiltonian in the form $\hat{H} = -2J\hat{S}_1\cdot\hat{S}_2 + g\mu_B(S_1 + S_2)\cdot B$ was used. Simulation of the experimental magnetic data with a full-matrix diagonalization of exchange coupling and Zeeman splitting was performed with the julX program (E. Bill, Max-Planck-Institut für Bioanorganische Chemie, Mülheim an der Ruhr, Germany). Before simulation, the experimental data were corrected for the underlying diamagnetism by using tabulated Pascal constants (incremental method) and for temperature-independent paramagnetism (*TIP*). A Curie–Weiss-behaved paramagnetic impurity (*PI*) with spin $S = 5/2$ was included according to $\chi = (1 - PI)\cdot\chi + PI\cdot\chi_{mono}$. Best fit parameters for **1**: $J = -180\ cm^{-1}$, $g = 2.000$ (fixed), $PI = 1.7\%$, $\chi(TIP) = 35.3 \times 10^{-6}\ cm^3\,mol^{-1}$; for **2**: $J = -158\ cm^{-1}$, $g = 2.000$ (fixed), $PI = 0.9\%$, $\chi(TIP) = 10.1 \times 10^{-6}\ cm^3\,mol^{-1}$; for **3**: $J = -141\ cm^{-1}$, $g = 2.016$ (fitted), $PI = 9.0\%$, $\chi(TIP) = 20.1 \times 10^{-6}\ cm^3\,mol^{-1}$.

Received: January 28, 2009
Published Online: May 13, 2009

  